Acta Crystallographica Section B
Structural Science
ISSN 0108-7681

Charge density study of hydrogen [(2,4-diaminopyrimidin-1-io)methyl]phosphonate monohydrate

Miroslav Slouf,[a]* Antonin Holy,[b] Vaclav Petricek[c] and Ivana Cisarova[a]

[a]Department of Inorganic Chemistry, Charles University, Hlavova 2030, 128 40 Praha 2, Czech Republic, [b]Institute of Organic Chemistry and Biochemistry, Academy of Sciences of the Czech Republic, Flemmingovo 2, 166 10 Praha 6, Czech Republic, and [c]Institute of Physics, Academy of Sciences of the Czech Republic, Na Slovance 2, 182 21 Praha 8, Czech Republic

Correspondence e-mail: slouf@imc.cas.cz

Received 29 October 2001
Accepted 1 March 2002

The crystal structure and charge density of hydrogen (2,4-diaminopyrimidin-1-io)methyl]phosphonate monohydrate, $C_5H_9N_4O_3P\cdot H_2O$, have been determined by means of single-crystal X-ray diffraction. Diffraction data were collected at 105 K with Mo $K\alpha$ radiation to a resolution of $\sin\theta/\lambda = 1.08$ Å^{-1}. A four-circle diffractometer equipped with a CCD area detector was used to collect 50 161 reflections over 3 d. 6082 unique reflections with $I > 3\sigma(I)$ were used in the multipole model to map the deformation electron density and gave the final statistical factors $R(F) = 0.0329$, $wR(F) = 0.0235$ and g.o.f. = 1.37. Structure determination revealed that two O atoms in the crystal structure of the title compound act as hydrogen-bond acceptors for more than one hydrogen bond. Examination of deformation electron density maps showed preferential polarization of the lone-pair electron density of the two O atoms into the shortest hydrogen bonds.

1. Introduction

Studies of charge density distribution in crystals require accurate, high-angle and low-temperature diffraction data (Coppens, 1998). Several recent publications prove that such data can be obtained using area detectors (Martin & Pinkerton, 1998; Dahaoui *et al.*, 1999; Volkov *et al.*, 1999 *etc*). In this work, the charge density distribution of an organic compound, hydrogen-[(2,4-diaminopyrimidin-1-io)methyl]-phosphonate monohydrate (HPPM), was obtained from data collected on a CCD-equipped diffractometer. HPPM crystallizes in the monoclinic system [$a = 5.8389$ (2), $b = 19.3579$ (5), $c = 8.0338$ (3) Å and $\beta = 97.203$ (2)°] with centrosymmetric space group $P2_1/n$ (No. 14). Data collection took less than 3 d. The equivalent diffraction data would have been collected for several weeks on a conventional diffractometer with point detector.

HPPM belongs among acyclic nucleoside phosphonates (ANP), which are isopolar analogs of nucleotides. ANP contain the phosphonomethyl ether function linked to the aliphatic side chain of *N*-alkylpurine or -pyrimidine, replacing the phosphoric acid ester residue bound to the nucleoside sugar moiety. These compounds attract much attention owing to their antiviral and cytostatic activity. We have performed a detailed study of the antiviral activity of the so-called PME series of ANP [purine or pyrimidine 2-(phosphonomethoxy)-ethyl derivatives] (Holy, Gunter *et al.*, 1999). It resulted in the formulation of the pharmacofor that is characterized by the cumulation of amino groups at the pyrimidine ring of the purine base. This led to an investigation of PME derivatives

derived from 2,4-diaminopyrimidine and related compounds. The structure of the parental compound of this series, quaternary hydrogen[2-(2,4-diaminopyrimidin-1-io)ethoxymethyl]phosphonate, was characterized by X-ray analysis (Holy, Budesinsky *et al.*, 1999). This paper deals with a related simplified zwitter-ionic compound HPPM, in which the 2,4-diaminopyrimidine is quaternized by phosphonomethyl function only, thus preserving the zwitterionic character of the molecule. HPPM was prepared by reaction of 2,4-diaminopyrimidine with diisopropyl tosyloxymethylphosphonate followed by removal of protecting phosphonate ester groups *via* transsilylation with bromotrimethylsilane and hydrolysis. HPPM was isolated by ion exchange chromatography.

2. Synthesis and crystallization

The synthesis and preliminary characterization of HPPM was performed as follows: a mixture of 2,4-diaminopyrimidine (3.3 g, 30 mmol) and diisopropyl tosyloxymethylphosphonate (11.4 g, 32 mmol; Holy, 1993) in dimethylformamide (25 ml) was heated for 16 h at 383 and the solvent evaporated *in vacuo*. Acetonitrile (40 ml) and bromotrimethylsilane (20 ml) were added to the residue and the mixture was stirred overnight at ambient temperature under the exclusion of moisture. The volatiles were evaporated *in vacuo*, the residue codistilled with acetonitrile (2 × 50 ml) and dissolved in dilute (1:20) aqueous ammonia. The solution was evaporated *in vacuo*, the residue in concentrated aqueous solution was alkalized with concentrated ammonia to pH 10 and applied on a Dowex 1 X 2 (acetate form) column (200 ml). The column was washed with water (3 ml min^{-1}) until the UV absorption (at 260 nm) of the eluate dropped and then washed with 0.1 *M* acetic acid. The UV-absorbing acid eluate was evaporated *in vacuo*, the residue was co-distilled twice with water (50 ml each) and crystallized from water. Yield: 2.0 g (30.0%), m.p. 603 K. For $C_5H_9N_4O_3P{\cdot}H_2O$ (222.14) calculated C 27.03, H 4.99, N 25.22, P 13.94%; found C 26.99, H 5.04, N 25.05, P 13.67%. Mass spectrum: MH 205.

^{1}H NMR (in D_2O + NaOD; 500 MHz): 7.58 d, 1 H [H-6, J(6,5) = 7.4 Hz]; 6.08 d, 1H [H-5, J(5,6) = 7.4 Hz (H-1′)]; 3.81 d, 2H [H-1′, J(1′,P) = 11.0 Hz]. ^{13}C NMR (in D_2O + NaOD; 125.7 MHz): 166.75 s (C-2); 159.93 s (C-4); 100.63 s (C-5); 149.54 s (C-6); 54.00 d, J(C,P) = 130.4 Hz (C-1′).

Crystals of HPPM suitable for charge-density analysis were grown using the thermal gradient method. A small amount of the crystalline powder of HPPM (∼5 mg) was dissolved in a minimal amount of boiling water (∼0.5 ml). The solution in the closed vial was placed immediately into the thermos flask filled with boiling water. The thermos flask was left to equilibrate at room temperature for 3 d, after which the crystals appeared. They were colourless, transparent prisms with approximate dimensions from 0.05 to 0.5 mm.

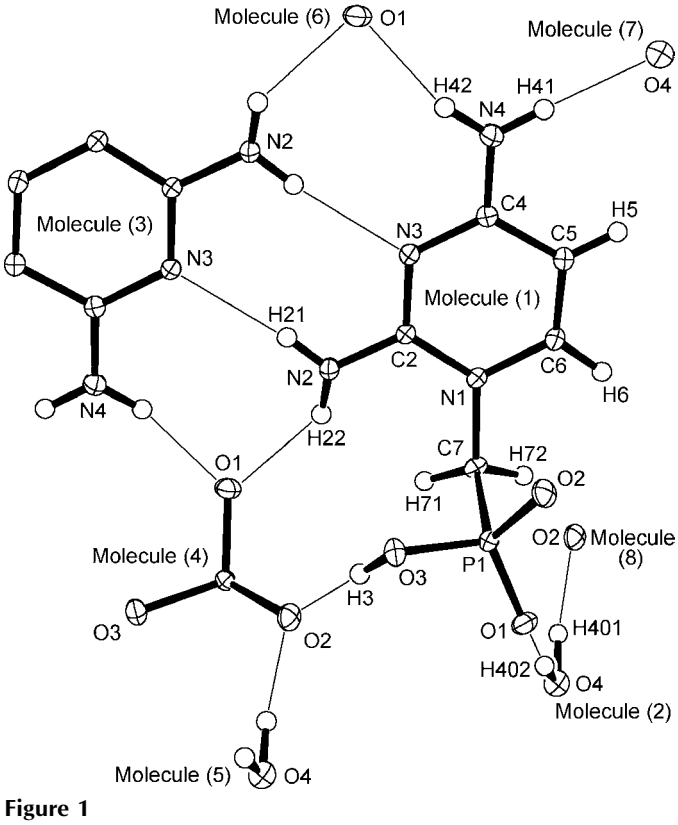

Figure 1
*ORTEP*II (Johnson, 1976; Farrugia, 1997) view of the packing of $C_5H_9N_4O_3P{\cdot}H_2O$. The thermal displacement ellipsoids of the non-H atoms are drawn at the 50% probability level. Hydrogen bonds are indicated by thin lines. Symmetry codes: (1), (2) x, y, z; (3) $-x+1, -y+1, -z+2$; (4) $x+\frac{1}{2}, y-\frac{1}{2}, z+\frac{1}{2}$; (5) $x+1, y, z$; (6) $-x+\frac{1}{2}, y+\frac{1}{2}, -z+\frac{3}{2}$; (7) $-x-\frac{1}{2}, y+\frac{1}{2}, -z+\frac{3}{2}$; (8) $x-\frac{1}{2}, -y+\frac{1}{2}, z+\frac{1}{2}$.

3. Data collection and data reduction

Room temperature, low-angle ($\sin\theta_{max}/\lambda$ = 0.6 $Å^{-1}$) data collection was used to determine the structure of HPPM and to check crystal quality. It was found that the HPPM is monoclinic ($a \simeq 5.8$, $b \simeq 19.4$, $c \simeq 8.0$ Å and $\beta \simeq 97.2°$), with the centrosymmetric space group $P2_1/n$ (No. 14), diffracting well in the high-angle region ($\sin\theta/\lambda > 0.8$ $Å^{-1}$). The expected molecular structure (Fig. 1) was confirmed. The final statistical factor $R(F)$ = 0.0315 indicated that the crystal quality might be sufficient for charge density analysis.[1]

Data for the charge density study were collected as follows. A good quality crystal (0.2 × 0.2 × 0.3 mm) was fixed on a glass fibre with silicon grease, mounted on the goniometer head of a Nonius KappaCCD diffractometer equipped with a two-dimensional CCD detector (diameter 6.35 cm, pixel-to-millimetre ratio 9.1) and conventional X-ray tube (Mo $K\alpha$ radiation, λ = 0.71073 Å). The crystal was cooled at 105 K with a Oxford Cryostream liquid nitrogen cooler using the cooling rate 120 K h^{-1}. Data collection was controlled by the program *COLLECT* (Hooft, 1998). Fast preliminary data collection showed that the crystal diffracted with observable intensities up to θ_{max} = 50°, which corresponded to $\sin\theta_{max}/\lambda$ = 1.08 $Å^{-1}$. Indexation of a few reflections with *DENZO* (Otwinowski & Minor, 1997) confirmed the unit-cell para-

[1] Supplementary data for this paper are available from the IUCr electronic archives (Reference: LC0047). Services for accessing these data are described at the back of the journal.

Table 1
Experimental details.

Crystal data	
Chemical formula	$C_5H_9N_4O_3P{\cdot}H_2O$
Chemical formula weight	222.15
Cell setting, space group	Monoclinic, $P2_1/n$
a, b, c (Å)	5.8389 (2), 19.3579 (5), 8.0338 (3)
β (°)	97.203 (2)
V (Å^3)	900.88 (5)
Z	4
D_x (Mg m^{-3})	1.638
Radiation type	Mo $K\alpha$
No. of reflections for cell parameters	21 482
θ range (°)	1–50
μ (mm^{-1})	0.303
Temperature (K)	105.0 (1)
Crystal form, colour	Prism, translucent colourless
Crystal size (mm)	0.3 × 0.2 × 0.2
Data collection	
Diffractometer	Nonius KappaCCD
Data collection method	CCD rotation scans
No. of measured, independent and observed reflections	34 544, 9362, 6076
Criterion for observed reflections	$I > 3\sigma(I)$
R_{int}	0.037
θ_{max} (°)	50.52
Range of h, k, l	$0 \rightarrow h \rightarrow 12$ $0 \rightarrow k \rightarrow 42$ $-17 \rightarrow l \rightarrow 16$
Refinement	
Refinement on	F
R, wR, S	0.0329, 0.0215, 1.37
No. of reflections and parameters used in refinement	9362, 368
H-atom treatment	Mixed
Weighting scheme	$w = 1/\sigma^2(F)$
$(\Delta/\sigma)_{max}$	0.0028
$\Delta\rho_{max}$, $\Delta\rho_{min}$ (e Å^{-3})	0.93, −1.25
Extinction method	Isotropic
Extinction coefficient	0.026 (2)

meters and monoclinic crystal system. Data collection was divided into two steps in order to improve $I/\sigma(I)$ ratios for weak, high-angle reflections. The low-angle data (θ_{max} = 35°, sin θ_{max}/λ = 0.81 Å^{-1}) were collected using lower exposure (112 s per frame) and high-angle data (θ_{max} = 50°, sin θ_{max}/λ = 1.08 Å^{-1}) were collected at higher exposure (420 s per frame). The average redundancy of the low-angle data was 2 and the average redundancy of the high-angle data was 1. A total of 15 sets of frames (framesets) were collected using φ and ω scans. The first eight framesets contained low-angle data and the last seven framesets contained high-angle data. A total of 876 collected frames contained 34 544 reflections. The data were 99.8% complete to 35° of θ and 96.9% complete to 50° of θ. The whole data collection took a little more than 3 d. The rotation per frame was 1.4°. The data collection strategy described above was dictated by hardware limitations: the higher redundancy or lower rotation per frame could not be used because it would have lead to a higher number of frames, which would not have fit into the memory of the computer controlling the diffractometer. Higher redundancy would have increased the precision of the measured intensities of all the reflections. Lower rotation per frame combined with higher exposure would have increased the precision for low-intensity reflections in the high-angle region. Data collection strategies based on higher redundancies (∼5 or even more measurements per reflection) and lower rotations per frame (∼0.2–0.3°) are usually used (Dahaoui *et al.*, 1999; Kuntzinger *et al.*, 1999; Volkov *et al.*, 1999, 2000).

The collected reflections were integrated with the program *DENZO*, which is part of an *HKL* program package (Otwinowski & Minor, 1997). The unit-cell parameters were refined by the program *SCALEPACK*, which is also part of the *HKL* program package. 21 482 of the strong reflections were used to refine the unit cell and confirmed that it was monoclinic, a = 5.8389 (2), b = 19.3579 (5), c = 8.0338 (3) Å and β = 97.203 (2)°. The space group $P2_1/n$ was determined from reflection intensities without ambiguity. Data reduction was performed with the program *SCALEPACK* in three steps. This three-step procedure was forced by the fact that 15 framesets were measured, whereas the *SCALEPACK* program is able to process 10 framesets in one run at most. In the first step, the first eight framesets were scaled, corrected for Lorentz and polarization effects and merged in the Laue group 2/*m* with the program *SCALEPACK* and the output file containing the reflections was saved. In the second step the last eight framesets were scaled, corrected for Lorentz and polarization effects, and merged in Laue group 2/*m* with the program *SCALEPACK* and the output file containing the reflections was saved as well. At the end both files containing the reflections were merged and scaled with the program *SCALEPACK*, the final output file containing all the reflections. The absorption correction was neglected (μ = 0.303 mm^{-1}). The final data set contained 9362 independent reflections, 6082 of which were observed [$I > 3\sigma(I)$]. The internal agreement factor was R_{int} = 0.037 and R_σ = 0.038.[2] The table showing resolution *versus* numbers of reflections and agreement factors is given in the supplementary material. Experimental details are summarized in Table 1.

4. Refinement

The structure was determined by direct methods using *SIR*92 (Altomare *et al.*, 1994). The conventional refinement was performed with the program *JANA*2000 (Petricek & Dusek, 2000). One molecule of hydrogen {2-(2,4-diaminopyrimidin-1-io)methyl}phosphonate and one molecule of water were found in the asymmetric unit (Fig. 1). All non-H atoms were refined anisotropically and H atoms were refined isotropically. The

[2] Definition of agreement factor symbols used in this article: R_{int} is the residual $\Sigma|\mathrm{av}(\Delta I)|/\Sigma|\mathrm{av}(I)|$ for symmetry-equivalent reflections used to calculate the average intensity av(I); the $|\mathrm{av}(\Delta I)|$ term is the average absolute difference between av(I) and the individual symmetry equivalent intensities. R_σ is the measure $\Sigma|u(\mathrm{net}I)|/(|\mathrm{net}I|)$ for all the measured reflections. $R(F) = \Sigma||F_{obs}| - |F_{calc}||/|F_{obs}|$, where F_{obs} are the observed structure-factor amplitudes, F_{calc} are the calculated structure-factor amplitudes and the summation runs through the observed reflections. $wR(F) = (\Sigma w(|F_{obs}| - |F_{calc}|)^2/\Sigma w|F_{obs}|^2)^{1/2}$, where F_{obs}, F_{obs}, F_{calc} are defined above, w is the least-squares reflection weight and the summation runs through observed reflections. g.o.f. = $(\Sigma w(|F_{obs}| - |F_{calc}|)^2/(N_{ref} - N_{param}))^{1/2}$, where F_{obs}, F_{calc} and w are defined above, N_{ref} is the number of reflections used in the refinement, N_{param} is the number of refined parameters and summation runs through all the reflections.

Table 2
Results of rigid-bond test (Hirshfeld, 1976) applied on the data from conventional, high-order and multipole refinement.

$Z^2_{A,B}$ and $Z^2_{B,A}$ are mean-square vibration amplitudes of atoms A and B along their mutual bond. ΔZ is the difference between $Z^2_{A,B}$ and $Z^2_{B,A}$.

		Conventional refinement			High-order refinement			Multipole refinement		
Atom A	Atom B	$Z^2_{A,B}$ (Å^2)	$Z^2_{B,A}$ (Å^2)	ΔZ (Å^2)	$Z^2_{A,B}$ (Å^2)	$Z^2_{B,A}$ (Å^2)	ΔZ (Å^2)	$Z^2_{A,B}$ (Å^2)	$Z^2_{B,A}$ (Å^2)	ΔZ (Å^2)
P1	O1	0.0101	0.0104	0.0004	0.0103	0.0112	0.0009	0.0102	0.0103	0.0001
P1	O2	0.0105	0.0110	0.0005	0.0105	0.0107	0.0002	0.0105	0.0100	0.0005
P1	O3	0.0101	0.0109	0.0008	0.0102	0.0110	0.0008	0.0104	0.0101	0.0003
P1	C7	0.0104	0.0129	0.0025	0.0106	0.0106	0.0001	0.0106	0.0113	0.0007
N1	C2	0.0092	0.0098	0.0006	0.0087	0.0085	0.0002	0.0083	0.0086	0.0002
N1	C6	0.0120	0.0123	0.0003	0.0113	0.0112	0.0001	0.0112	0.0111	0.0001
N1	C7	0.0101	0.0096	0.0005	0.0106	0.0110	0.0004	0.0101	0.0107	0.0006
N2	C2	0.0106	0.0122	0.0015	0.0093	0.0092	0.0001	0.0091	0.0094	0.0002
N3	C2	0.0102	0.0113	0.0011	0.0096	0.0101	0.0005	0.0095	0.0099	0.0004
N3	C4	0.0105	0.0117	0.0012	0.0096	0.0105	0.0009	0.0096	0.0101	0.0005
N4	C4	0.0114	0.0122	0.0008	0.0103	0.0106	0.0003	0.0103	0.0104	0.0001
C4	C5	0.0124	0.0117	0.0007	0.0106	0.0109	0.0002	0.0108	0.0105	0.0003
C5	C6	0.0143	0.0152	0.0010	0.0128	0.0132	0.0004	0.0129	0.0132	0.0003
Average value of $\sigma(u^2)$		~ 0.0002 Å^2			~ 0.0002 Å^2			~ 0.0002 Å^2		
R.m.s. discrepancy		$= 0.0011$ Å^2			$= 0.0005$ Å^2			$= 0.0004$ Å^2		

refinements were based on F and performed against all 9362 reflections. Convergence was achieved at $R(F) = 0.0465$, $wR(F) = 0.0461$ and g.o.f = 2.72.

The charge density distribution in the crystal was described by means of multipole refinement. It is a least-squares refinement technique based on a multipole model (Hansen & Coppens, 1978), in which the electron density of an atom is described by

$$\rho_{\rm atom}(\mathbf{r}) = \rho_{\rm core}(r) + P_v\kappa^3\rho_{\rm valence}(\kappa r) + \sum_{l=0}^{l_{\rm max}} \kappa'^3 R_l(\kappa' r) \sum_{m=0}^{l} P_{lm\pm} d_{lm\pm}(\theta, \varphi),$$

where the functions $\rho_{\rm core}$ and $\rho_{\rm valence}$ are the spherically averaged core and valence electron density, R_l represents the Slater-type radial density functions and $d_{lm\pm}$ are the multipolar spherical harmonic functions in the real form. The coordinates r, θ and φ refer to the local atom-centred Cartesian axes, which are defined by the user on each atom. Parameters P_v, $P_{lm\pm}$, κ and κ', describing the aspherical features of atomic electron density, are treated as new variables in the least-squares refinement. The valence-shell population parameter P_v gives the number of valence shell electrons. The multipolar population parameters $P_{lm\pm}$ describe the non-sphericity of atomic electron density. Expansion/contraction parameters κ and κ' are connected with the expansion and contraction of the perturbed density.

Multipole refinement was performed using the *JANA*2000 (Petricek & Dusek, 2000) crystallographic computing system, which was extended by V. Petricek to enable multipole refinement as defined in the program *MOLLY* (Hansen & Coppens, 1978). During multipole refinement two problems occurred. The first problem consisted in the fact that κ' parameters could not be refined simultaneously with multipolar parameters $P_{lm\pm}$ due to the large correlations that led to the instability of the least-squares procedure. The largest correlation was observed for κ'(O2) and P_{20}(O2). The second problem was connected with H-atom positions and displacement parameters, which had to be estimated from the X-ray diffraction data. In such a case it is usually not possible to refine displacement parameters $U_{\rm iso}$ and radial parameters κ simultaneously (Coppens *et al.*, 1979). However, the refinement could be carried out using the multi-step procedure whose description follows. After conventional least-squares refinement, the high-order refinement was performed using the reflections ($0.80 < \sin\theta/\lambda < 1.08$ Å^{-1}) to obtain the best estimate of atomic positions and displacement parameters of the non-H atoms. H-atom positional and displacement parameters were fixed during the high-order refinement. At the end of the high-order refinement the H atoms were shifted along the X—H bond vectors (where X is the relevant heavy atom) to average bond-distance values determined from neutron diffraction studies (Allen, 1986; *International Tables for Crystallography*, 1995). The bond distances used were 1.085 Å for Csp^3—H, 1.076 Å for Csp^2—H, 1.032 Å for N—H, 0.960 Å for O(water)—H and 1.070 Å for PO—H. At the end of the high-order refinement, the rigid-bond test (Hirshfeld, 1976) was applied to non-H atoms using the program *PLATON* (Spek, 1990). The test yielded encouraging results: the maximum discrepancy $\Delta Z^2 = 0.0009$ Å^2 was found for the N3—C4 bond (Table 2). Then the multipole refinement was carried out using all reflections with the following strategy:

(i) P_v of all atoms + κ of non-H atoms;
(ii) P_v, $P_{lm\pm}$ of all atoms + κ of non-H atoms;
(iii) P_v, $P_{lm\pm}$, U^{ij} of all atoms + κ of non-H atoms;
(iv) P_v, κ of all atoms;
(v) P_v, κ' of all atoms;
(vi) P_v, $P_{lm\pm}$, U^{ij} of all atoms + κ of non-H atoms;
(vii) P_v, $P_{lm\pm}$, U^{ij} of all atoms + positions, κ of non-H atoms;
(viii) P_v, κ of all atoms + positions of non-H atoms;
(ix) P_v, κ' of all atoms + positions of non-H atoms;
(x) P_v, $P_{lm\pm}$, U^{ij} of all atoms + positions, κ of non-H atoms.

At each step the scale was refined and the refinement was cycled until convergence. An isotropic extinction type I correction with Gaussian mosaic distribution was applied in the last refinement cycles, based on the approximation that the

Table 3
Bond lengths and angles (Å, °).

P1—O1	1.5022 (4)	N3—C4	1.3455 (7)
P1—O2	1.5103 (5)	C4—N4	1.3272 (7)
P1—O3	1.5774 (5)	C4—C5	1.4328 (7)
P1—C7	1.8427 (5)	N4—H41	1.032
O3—H3	1.070	N4—H42	1.032
N1—C2	1.3706 (7)	C5—C6	1.3507 (7)
N1—C6	1.3793 (7)	C5—H5	1.076
N1—C7	1.4723 (7)	C6—H6	1.076
C2—N2	1.3326 (7)	C7—H71	1.085
C2—N3	1.3387 (7)	C7—H72	1.085
N2—H21	1.032	O4—H401	0.960
N2—H22	1.032	O4—H402	0.960
O1—P1—O2	116.30 (2)	N4—C4—C5	119.76 (4)
O1—P1—O3	112.33 (2)	C4—N4—H41	117.04
O1—P1—C7	108.53 (2)	C4—N4—H42	122.41
O2—P1—O3	107.08 (3)	H41—N4—H42	120.37
O2—P1—C7	106.19 (2)	C4—C5—C6	117.13 (4)
O3—P1—C7	105.75 (2)	C4—C5—H5	122.24
C2—N1—C6	118.67 (4)	C6—C5—H5	120.63
C2—N1—C7	123.43 (4)	N1—C6—C5	121.56 (5)
C6—N1—C7	117.43 (4)	N1—C6—H6	114.37
N1—C2—N2	120.38 (4)	C5—C6—H6	124.07
N1—C2—N3	122.05 (4)	P1—C7—N1	111.57 (3)
N2—C2—N3	117.57 (5)	P1—C7—H71	110.18
C2—N2—H21	115.73	P1—C7—H72	106.83
C2—N2—H22	124.10	N1—C7—H71	111.50
H21—N2—H22	119.19	N1—C7—H72	107.45
C2—N3—C4	119.47 (5)	H71—C7—H72	109.15
N3—C4—N4	119.18 (5)	H401—O4—H402	96.76
N3—C4—C5	121.05 (5)		

Table 4
Distances of selected atoms from the best plane through atoms N1, C2, N3, C4, C5 and C6 (Å).

Atom	Distance	Atom	Distance
N1	+0.010 (1)	H5	−0.032
C2	−0.007 (1)	H6	+0.010
N3	−0.006 (1)	N2	−0.030 (1)
C4	+0.016 (1)	H21	−0.121
C5	−0.014 (1)	H22	−0.148
C6	+0.002 (1)	N4	+0.051 (1)
C7	+0.209 (1)	H41	+0.079
		H42	+0.137

Table 5
Hydrogen-bonding geometry (Å, °).

D—H···A	$d(D$—H)	d(H···A)	$d(D\cdots A)$	$\angle DHA$
N2—H21···N3^{i}	1.032	1.954	2.9804 (7)	172.9
N2—H22···O1^{ii}	1.032	2.000	2.8729 (7)	140.6
N4—H41···O4^{iii}	1.032	1.807	2.8374 (7)	176.3
N4—H42···O1^{iv}	1.032	1.932	2.9392 (7)	164.4
O3—H3···O2^{ii}	1.070	1.474	2.5431 (7)	176.3
O4—H401···O2^{v}	0.960	1.782	2.7383 (8)	173.6
O4—H402···O1	0.960	1.809	2.7648 (7)	173.6

Symmetry codes: (i) $-x+1,-y+1-z+2$; (ii) $x+\frac{1}{2},-y+\frac{1}{2},z+\frac{1}{2}$; (iii) $-x-\frac{1}{2},y+\frac{1}{2},-z+\frac{3}{2}$; (iv) $-x+\frac{1}{2},y+\frac{1}{2},-z+\frac{3}{2}$; (v) $x-\frac{1}{2},-y+\frac{1}{2},z+\frac{1}{2}$.

crystal is a sphere with radius 0.1 mm. The extinction gave the final value of the extinction coefficient as 0.026 (2) and slightly improved the final agreement factors. Whenever the positions of the non-H atoms changed, the H atoms were adjusted so that the X—H bond distances were kept constant. The starting values of ζ and n_l coefficients, which are used to define the radial functions R_l, were obtained as described by Coppens (1997*a*). The starting values of radial parameters κ and κ' for the non-H atoms were 1.0 and for the H atoms they were 1.2. The H atoms were divided into three groups in which the values of P_v, κ and κ' parameters were kept equal. The first group contained all H atoms bound to C atoms, the second group contained all H atoms bound to N atoms and the last group contained all H atoms bound to O atoms. Multipolar expansion was truncated at the octupolar level for the non-H atoms and at the dipolar level for the H atoms. The multipole population parameters $P_{lm\pm}$ of the aromatic ring atoms N1, C2, N3, C4, C5 and C6 were constrained to obey local mirror-plane symmetry, the mirror-plane being the aromatic ring plane. The multipole population parameters $P_{lm\pm}$ of the water molecule O4 atom were constrained to obey mirror plane symmetry, the mirror plane going through the O atom and bisecting the plane of the water molecule. All H atoms were given cylindrical symmetry, which means than just one dipolar parameter P_{10} of each atom was refined. P_v, $P_{lm\pm}$, κ and κ' parameters of the converged model have been deposited as supplementary material, together with all other relevant crystallographic data. The final values of statistical factors were $R(F) = 0.0329$, $wR(F) = 0.0235$ and g.o.f. = 1.37. The rigid-bond test performed at the end of multipole refinement yielded very good results, as documented in Table 2. This proves that displacement parameters of non-H atoms were successfully deconvoluted from the electron density parameters and confirms the correctness of the model.

5. Results and discussion

An *ORTEP* (Johnson, 1976) view of the symmetric unit of HPPM is shown in Fig. 1. Atomic coordinates and isotropic displacement parameters have been deposited as supplementary material. Selected geometric parameters are given in Tables 3–5. Anisotropic thermal displacement parameters and charge density parameters P_v, κ, $P_{lm\pm}$ and κ' are also given as supplementary material. The aromatic ring formed by N1, C2, N3, C4, C5 and C6 is planar. Both $-NH_2$ groups bound to the ring are also planar, being located in the plane of the ring (Table 4). The C7 atom is somewhat displaced out of the ring plane. The distance of the C7 atom from the best plane through atoms N1, C2, N3, C4, C5 and C6 is 0.209 (1) Å. The angle between the aromatic ring plane and the N1—C7 bond is 8.2°. The bulky $-PO_3H^-$ group is located outside the ring plane. The angle between the aromatic ring plane and the plane defined by the atoms N1, C7 and P1 is 88.8°. The molecules in the crystal are linked by a complex system of hydrogen bonds. All the H atoms bound to the O and N atoms are involved in the hydrogen bonding (Table 5).

Electron densities in the aromatic ring plane are given in Fig. 2. On the dynamic deformation density map (Fig. 2*a*), all bonding features, including the lone-pair orbital on the N3 atom, are clearly visible. The average electron density in the C—C bonding peaks of the aromatic ring is 0.60 e Å^{-3} and the

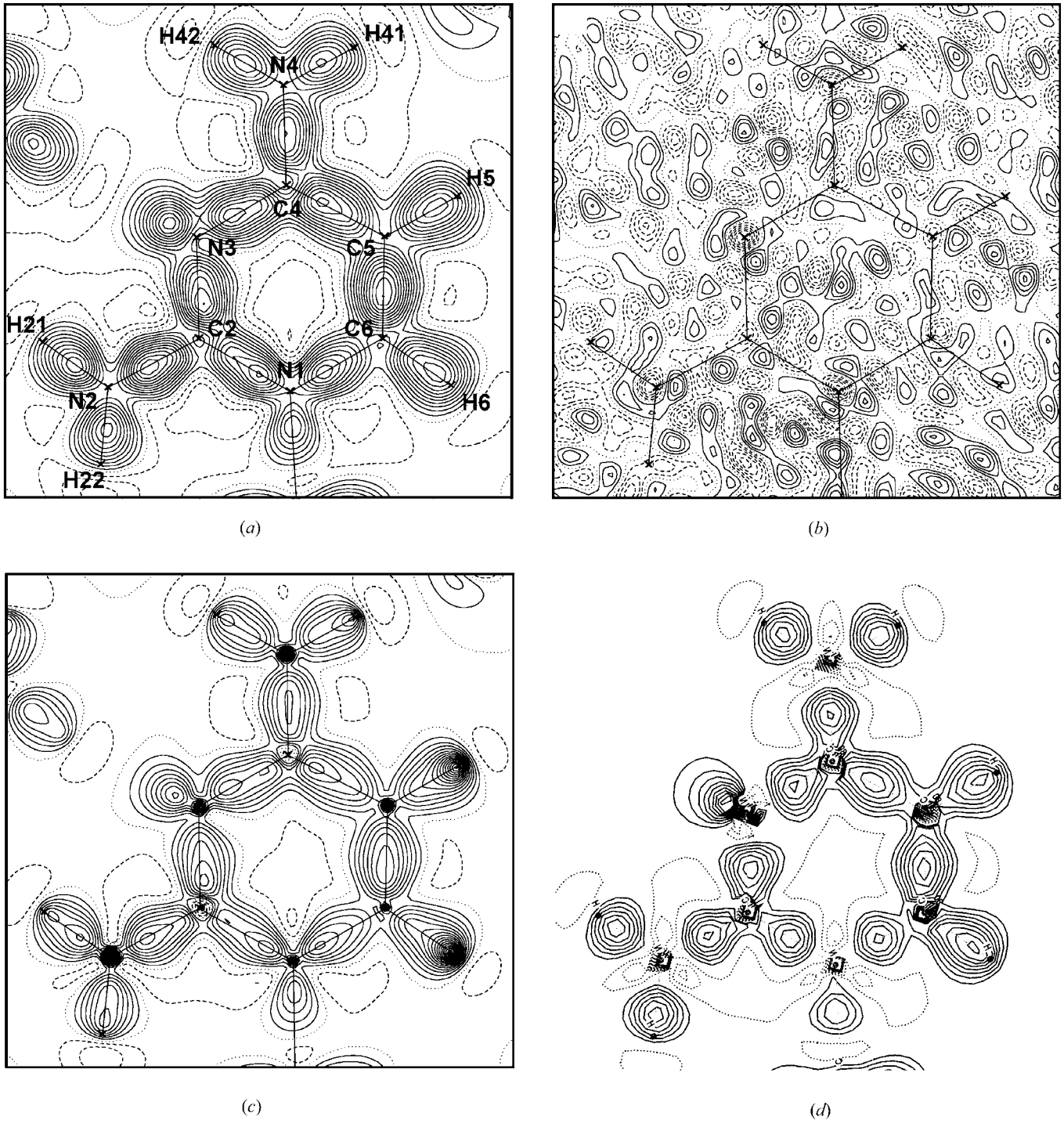

Figure 2
Electron density map of the aromatic ring of $C_5H_9N_4O_3P{\cdot}H_2O$. Positive, zero and negative contours are full, dotted and dashed lines, respectively. (*a*) Dynamic model deformation electron density map, contours at 0.05 e Å^{-3}; (*b*) residual map at the end of multipole refinement, contours at 0.1 e Å^{-3}; (*c*) static model deformation electron density map, contours at 0.1 e Å^{-3}; (*d*) theoretical HF/6-31G** map, contours at 0.1 e Å^{-3}, zero contour omitted, negative contours dotted.

average electron density of the C—N bonding peaks of the aromatic ring is 0.50 e Å^{-3}. These results agree quite well with previous X-ray diffraction studies (Stevens *et al.*, 1978; Epstein *et al.*, 1982; Swaminathan *et al.*, 1985; Souhassou *et al.*, 1991; Dahaoui *et al.*, 1999). The residual density map (Fig. 2*b*) shows a relatively high maxima and minima, but the noise does not seem to have influenced the model deformation electron density maps (Figs. 2*a* and *c*), because they work as noise filters (Coppens, 1997*b*). The static deformation electron density map (Fig. 2*c*) and theoretical *ab initio* HF/6-31G** map (Fig. 2*d*) show quite good agreement; bonding peaks among non-H atoms and the lone-pair peak of the N3 atom

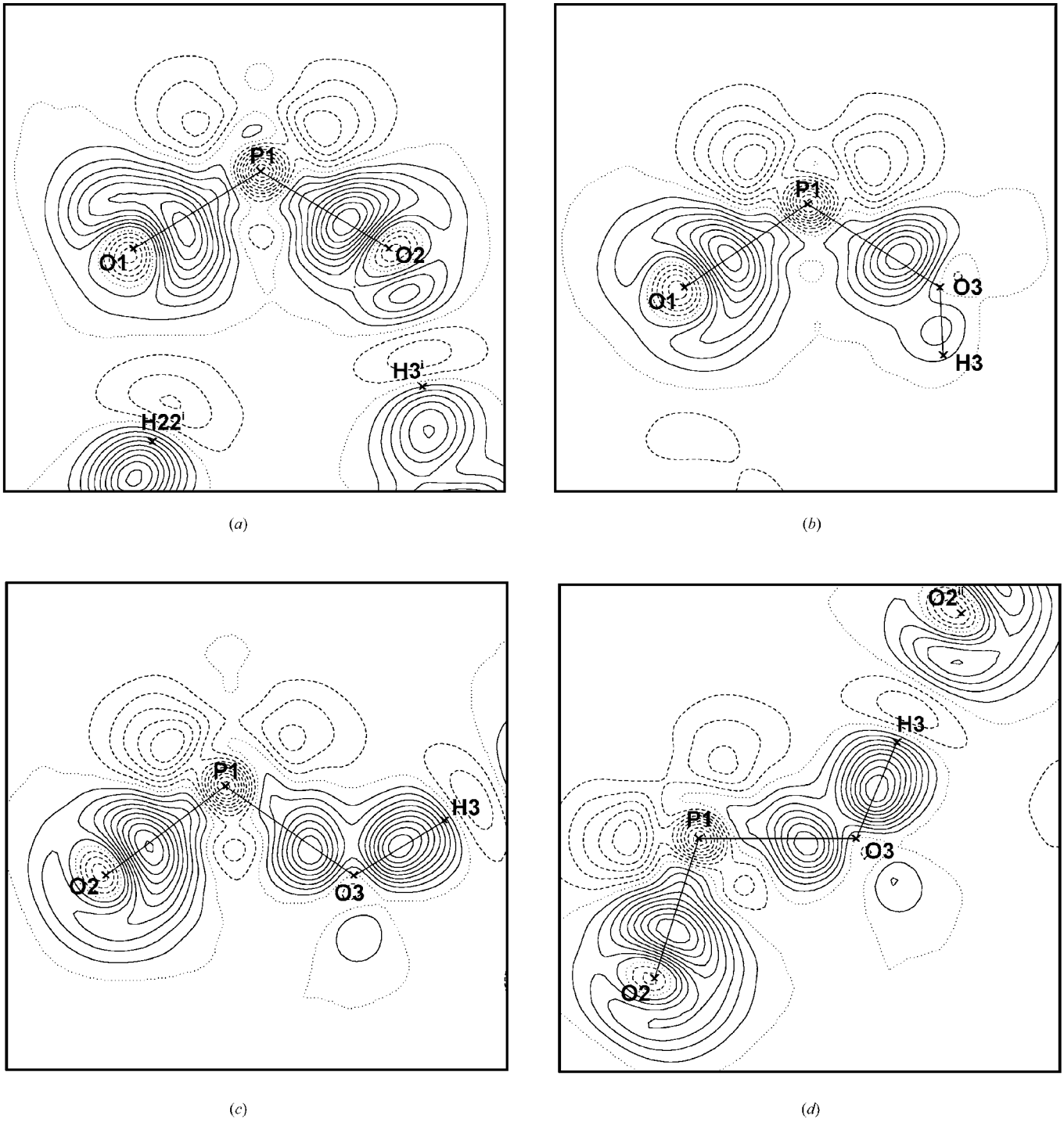

Figure 3
Dynamic model deformation electron density map of P—O bonds. (*a*) O1—P1—O2 plane; (*b*) O1—P1—O3 plane; (*c*) O2—P1—O3 plane; (*d*) P1—O3—H3 plane. Symmetry codes: (i) $x-\frac{1}{2}, -y+\frac{1}{2}, z-\frac{1}{2}$; (ii) $x+\frac{1}{2}, -y+\frac{1}{2}, z+\frac{1}{2}$. Contours at 0.5 e Å^{-3}.

agree within one contour level. On the other hand, there are also some differences: the positions of the bonding peaks between atoms on the static map are not quite identical with those on the HF/6-31G** map; N1—C2 and N3—C4 bonding peaks are split on the static map and the electron density near H atoms is too high on the static map. Discrepancies between the dynamic and HF/6-31G** map are lower, which suggests that the above-mentioned features of the static map were not correct and that those features were compensated for by thermal displacement parameters in part. Theoretical HF-6-31G** maps were calculated with the programs *GAUSSIAN*94 (Frisch *et al.*, 1995) and *MOLDEN* (Schaftenaar & Noordik, 2000).

Fig. 3 shows the dynamic deformation electron density of P—O bonds. The average density of P—O bonding peaks is 0.45 e Å^{-3} and the density of the P—OH bonding peak is

0.35 e Å^{-3}, which is comparable with previous studies (Pearlman & Kim, 1985; Souhassou *et al.*, 1995; Espinosa *et al.*, 1996; Pérès *et al.*, 1999). The higher peak height of P—O bonds in comparison with the P—OH bond is in accordance with the expected double-bond and single-bond characters, respectively (Ichikawa *et al.*, 1998). Also, the electron deficiency (−0.15 to −0.35 e Å^{-3}) at the opposite side of phosphorus relative to each P—O bond was observed in previous studies (Ichikawa *et al.*, 1998). In the work of Souhassou *et al.* (1995), the experimental deformation electron density maps of P—O bonds show small, sharp peaks around O atoms, which are not observed clearly here. The same peaks were observed on theoretical deformation electron density maps calculated by Moss *et al.* (1995). The major discrepancy between this work on one side and previous experimental and theoretical studies on the other side is the electron density of the lone-pair peak of the O3 atom, which is involved in the P—OH bond. The electron density of the lone-pair peak is as low as 0.10 e Å^{-3} (Figs. 3*c* and *d*) and is clearly underestimated. However, the overall shape of the deformation electron density of the P—O bonds is comparable both with the earlier deformation-density work on phosphate-containing compounds listed above and with theoretical deformation electron density maps (Moss *et al.*, 1995; Slouf, 2001).

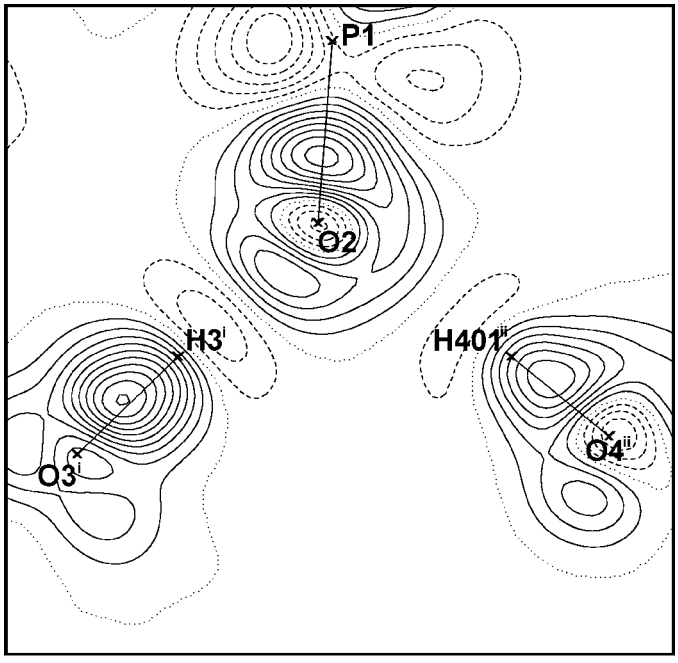

(*a*)

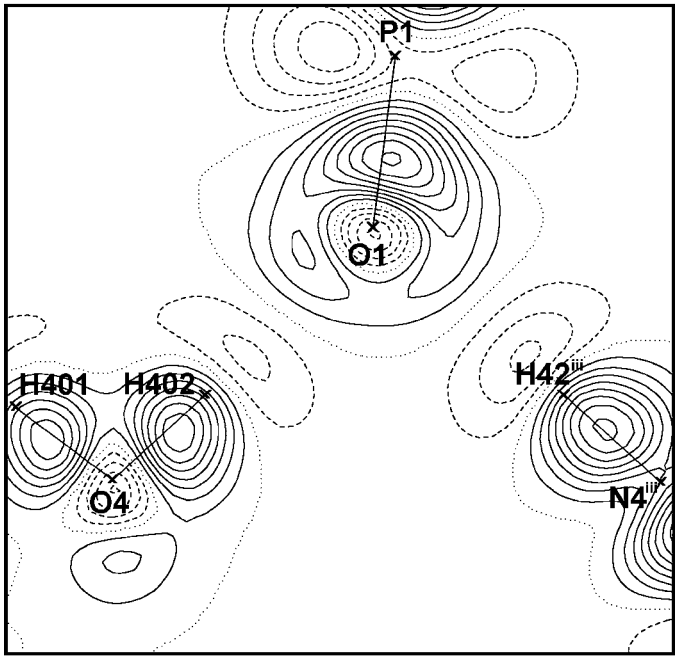

(*b*)

Figure 4
Dynamic model deformation electron density map showing hydrogen bonds with O1 and O2 acceptor atoms. (*a*) Acceptor atom O2, hydrogen bonds O3—H3···O2 and O4—H401···O2. Plot plane defined by atoms O2, H3^{i} and H401^{ii}. (*b*) Acceptor atom O1, hydrogen bonds O4—H401···O1 and N4—H42···O1. Plot plane defined by atoms O1, H401 and H42^{iii}. Symmetry codes: (i) $x-\frac{1}{2}, -y+\frac{1}{2}, z-\frac{1}{2}$; (ii) $x+\frac{1}{2}, -y+\frac{1}{2}, z-\frac{1}{2}$; (iii) $-x+\frac{1}{2}, y-\frac{1}{2}, -z+\frac{3}{2}$. Contours at 0.5 e Å^{-3}.

Fig. 4 shows the deformation electron density of atoms O1 and O2, which act as acceptors of three and two hydrogen bonds, respectively (Table 5). Fig. 4(*a*) shows two hydrogen bonds with the common acceptor atom O2. On the left side of Fig. 4(*a*) there is the shorter hydrogen bond O3—H3···O2, with the donor–acceptor distance *d*(O3···O2) = 2.5431 (7) Å. On the right side of Fig. 4(*a*) there is the longer hydrogen bond O4—H401···O2, with the donor–acceptor distance *d*(O4···O2) = 2.7383 (8) Å. The lone-pair electron density of O2 is polarized mostly in the direction of the stronger and shorter bond. A small polarization in the direction of the longer hydrogen bond is also observable. Such polarization of lone-pair electron density is in accordance with the charge density studies of hydrogen-bonding interactions in α-oxalic acid dihydrate (Stevens & Coppens, 1980; Stevens, 1980; Dam *et al.*, 1983). Oxalic acid dihydrate contains a short hydrogen

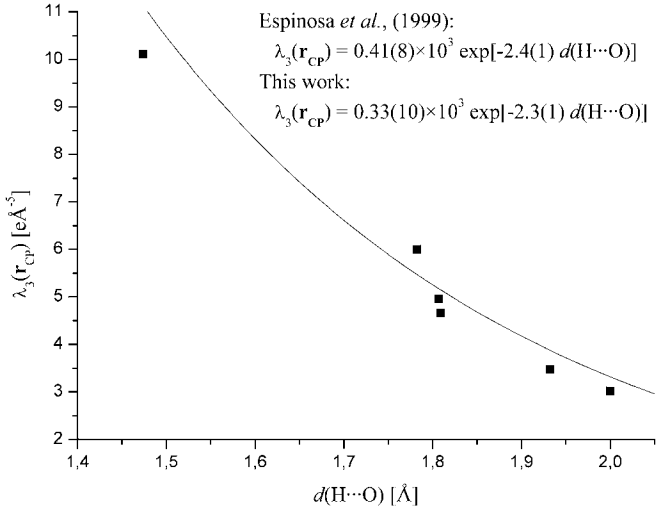

Figure 5
Phenomenological behaviour of λ_3 *versus* *d*(H···O).

Table 6
Topological characterization of covalent bond critical points.

The topological distance d_{AB} is the distance between atoms A and B (Å); distances d_A and d_B (Å) are the distances from the relevant (3, −1) critical point to atoms A and B, respectively. Values ρ_b (e Å^{-3}), $\nabla^2\rho_b$ (e Å^{-5}), ε (dimensionless) and λ_1, λ_2, λ_3 (e Å^{-5}) are electron density, its Laplacian, ellipticity and the three curvatures at the relevant (3, −1) critical point, respectively.

Atom A	Atom B	d_{AB}	d_A	d_B	ρ_b	$\nabla^2\rho_b$	ε	λ_1	λ_2	λ_3
P1	O1	1.5022 (4)	0.6132	0.8893	1.49	28.17	0.06	−9.96	−9.36	47.49
P1	O2	1.5103 (5)	0.6123	0.8981	1.50	27.10	0.04	−10.54	−10.15	47.79
P1	O3	1.5774 (5)	0.6345	0.9450	1.28	17.90	0.03	−7.52	−7.31	32.73
P1	C7	1.8427 (5)	0.7182	1.1247	1.09	−3.90	0.04	−4.88	−4.67	5.65
N1	C2	1.3706 (7)	0.7866	0.5841	2.19	−16.97	0.20	−18.78	−15.62	17.43
N1	C6	1.3793 (7)	0.8139	0.5655	2.12	−18.86	0.11	−16.73	−15.12	13.00
N1	C7	1.4723 (7)	0.8572	0.6154	1.64	−8.79	0.13	−11.44	−10.15	12.81
C2	N2	1.3326 (7)	0.5326	0.8002	2.44	−27.02	0.19	−22.21	−18.59	13.78
C2	N3	1.3387 (7)	0.5953	0.7440	2.41	−19.15	0.17	−20.64	−17.64	19.13
N3	C4	1.3455 (7)	0.7725	0.5732	2.35	−19.65	0.14	−19.77	−17.31	17.43
C4	N4	1.3272 (7)	0.5519	0.7754	2.44	−25.27	0.13	−20.95	−18.56	14.24
C4	C5	1.4328 (7)	0.7387	0.6942	2.00	−15.27	0.15	−15.06	−13.12	12.91
C5	C6	1.3507 (7)	0.6514	0.6994	2.34	−22.53	0.25	−18.38	−14.68	10.54
O3	H3	1.070	0.7384	0.3317	2.27	−14.06	0.03	−30.59	−29.82	46.35
O4	H401	0.960	0.7293	0.2308	2.33	−24.42	0.02	−37.04	−36.23	48.85
O4	H402	0.960	0.7158	0.2442	2.35	−32.01	0.02	−40.69	−39.90	48.58
N2	H21	1.032	0.7653	0.2668	2.11	−23.62	0.06	−28.78	−27.18	32.34
N2	H22	1.032	0.7455	0.2865	2.17	−25.38	0.08	−29.07	−26.87	30.56
N4	H41	1.032	0.7452	0.2869	2.14	−23.57	0.06	−27.90	−26.29	30.62
N4	H42	1.032	0.7443	0.2877	2.12	−23.25	0.06	−27.73	−26.05	30.54
C5	H5	1.076	0.6606	0.4154	1.98	−17.51	0.07	−19.43	−18.11	20.03
C6	H6	1.076	0.6607	0.4153	1.95	−17.09	0.07	−19.32	−18.07	20.30
C7	H71	1.085	0.6495	0.4355	1.85	−15.37	0.07	−17.06	−15.93	17.62
C7	H72	1.085	0.6427	0.4425	1.85	−15.67	0.09	−17.09	−15.72	17.14

Table 7
Topological characterization of hydrogen-bond critical points.

The topological distance d_{HA} is the distance between atoms H and A (Å); distances d_H and d_A (Å) are the distances from the relevant (3, −1) critical point to atoms H and A, respectively. Other symbols are as defined in Table 6; symmetry codes are as in Table 5; just the H···O hydrogen bonds are ordered by the d_{HA} distance

D—H···A	d_{HA}	d_H	d_A	ρ_b	$\nabla^2\rho_b$	ε	λ_1	λ_2	λ_3
N2—H22···O1^{ii}	2.000	0.751	1.278	0.12	2.03	0.25	−0.55	−0.44	3.02
N4—H42···O1^{iv}	1.932	0.660	1.279	0.13	2.41	0.10	−0.56	−0.51	3.47
O4—H402···O1	1.809	0.612	1.198	0.21	2.75	0.08	−0.99	−0.92	4.66
N4—H41···O4^{iii}	1.807	0.587	1.221	0.17	3.53	0.03	−0.72	−0.70	4.96
O4—H401···O2^{v}	1.782	0.626	1.157	0.26	3.24	0.02	−1.40	−1.37	6.00
O3—H3···O2^{ii}	1.474	0.423	1.130	0.30	7.18	5.74	−2.55	−0.38	10.11
N2—H21···N3^{i}	1.954	0.658	1.296	0.17	2.54	0.04	−0.78	−0.75	4.07

bond, linking the oxalic acid and water molecule, which has the O···O distance 2.481 Å. All experiments are in agreement that the lone-pair peak of the water-molecule O atom is polarized into the short hydrogen bond (Coppens, 1997*c*). In the recent work of Spackman *et al.* (1999) it was confirmed that hydrogen bonding causes complex polarizations at the acceptor atoms. Fig. 4(*b*) shows two hydrogen bonds with the common acceptor atom O1. The shorter hydrogen bond O4—H4···O1 has the donor–acceptor distance 2.7649 (7) Å. The longer hydrogen bond N4*a*—H42···O1 has the donor–acceptor distance 2.9393 (7) Å. Again the electron density on the acceptor atom O1 is polarized in the directions of both bonds and the stronger polarization is found in the direction of the shorter and stronger bond O4—H4···O1. Residual maps showing the same parts of space as in Figs. 3 and 4 are given in the supplementary material.

Topological analysis (Bader, 1990) of the experimental electron density was carried out with the program *JANA*2000 (Petricek & Dusek, 2000). Bond critical points were searched along all bonds (Table 6) and hydrogen-bonding interactions (Table 7). The results were found to be comparable with those obtained in previous studies of similar compounds (Klooster *et al.*, 1992; Howard *et al.*, 1995; Souhassou *et al.*, 1995; Moss *et al.*, 1995; Ichikawa *et al.*, 1998; Pérès *et al.*, 1999; Espinosa *et al.*, 1996, 1999). Nevertheless, some discrepancies were found as well:

(i) The values of electron density at BCP for P—O bonds (ρ_b = 1.49, 1.50 e Å^{-3} for P—O bonds and 1.29 e Å^{-3} for the P—OH bond) are somewhat smaller than those found in the previous studies (Espinosa *et al.*, 1996; Pérès *et al.*, 1999), where the values 1.46–1.98 e Å^{-3} were obtained.

(ii) BCP for the H3···O3 hydrogen bond is displaced out of the line connecting H3 and O3 atoms (d_{AB} = 1.474 Å, whereas $d_A + d_B$ = 1.533 Å) and the ellipticity value of the H3···O3 interaction is absurdly high (ε = 5.74); such an extreme value must have been caused by an error in the total electron density map, which led to the simultaneous overestimation of λ_1 and underestimation of λ_2.

On the other hand, several topological features were found, which are in accordance with theoretical predictions and/or previous studies:

(i) All bonds among atoms of the aromatic ring (N1, C2, N3, C4, C5, C6) and non-H atoms bound to the aromatic ring (N2, N4, C7) show higher values of ellipticity at the BCP than bonds between other atoms, which is in accordance with the expected aromatic character of these bonds. In the theoretical study of Bader *et al.* (1983) the ellipticity of the C—C bonds in ethane, benzene and ethylene increases from 0.0 to 0.23 to 0.45. These values correspond reasonably with the experimental values from this work. However, in the experimental study of L-dopa (Howard *et al.*, 1995), a higher value of the average ellipticity of the six C—C aromatic bonds (ε = 0.33) was obtained.

(ii) The highest ellipticity was found at the BCP of the C5—C6 bond (ε = 0.25), whereas the ellipticity of the C4—C5 bond was lower (ε = 0.15). According to the simple valence-bond

theory, the C5—C6 bond has strong double-bond character, while C4—C5 is better described as single. The same trend was observed in the study of Klooster *et al.* (1992), who studied 1-methyluracil, the compound with the aromatic ring very similar to that in HPPM.

(iii) The electron density at the BCP's of P—O bonds is higher than the electron density at the BCP of the P—OH bond, which is in accordance with the bond lengths and expected partial double-bond character of P—O bonds and the single-bond character of the P—OH bond.

(iv) The topological properties of hydrogen bonds correspond with the previous studies, whose results were summarized in the recent work of Espinosa *et al.* (1999). Hydrogen bonds in Table 7 are listed according to their H···O distances, where H is the hydrogen and O is the relevant oxygen acceptor atom; the bond with the nitrogen acceptor atom is at the end of the list. H···O interactions follow all the trends described by Espinosa *et al.* (1999) quite well. For instance, the values of ρ_b, $\nabla^2\rho_b$ and λ_3 decrease with increasing distance dO and with increasing distance d(H···O). Remarkably good agreement was observed for the d(H···O)–λ_3 relationship, as documented in Fig. 5. It is also in accordance with the conclusion of Espinosa *et al.* (1999) that the positive curvature λ_3 shows a very well defined behaviour *versus* d(H···O) in all X—H···O interactions.

Relatively large maxima and maxima ($\Delta\rho_{max}$ = +0.93, $\Delta\rho_{min}$ = −1.25 e Å^{-3}) were found on the residual maps; the highest minimum is found at the position of the P atom [d(P1-minimum) = 0.04 Å] and other extremes are located mostly around the P atom as well. Moreover, not all charge-density variables could be refined together during the multipole refinement. These facts indicate that the diffraction data were not of the highest quality. It is possible that the higher accuracy of reflection intensities might have been obtained using a higher redundancy and a lower rotation per frame combined with higher exposures, as recommended in the recent charge density studies based on CCD-equipped diffractometers (Martin & Pinkerton, 1998). On the other hand, the deformation electron density maps show all the bonding features, including the polarization of the lone-pair electron density due to hydrogen bonds, which suggests that the charge density in the crystal is well described by the final model. The results of the rigid-bond test and the average electron densities in bonding peaks confirm the correctness of the model as well. Satisfactory description of the charge density in the crystal could be achieved in this study on condition that suitable refinement strategy was applied.

Quantum chemistry calculations were performed with a virtual metacomputer built within the Metacenter project (http://meta.cuni.cz). M. Slouf would like to thank Professor Niels K. Hansen for his valuable pieces of advice concerning multipole refinement and to the Grant Agency of the Czech Republic for financial support (GACR 203/99/MO037). A. Holy is indebted to Dr M. Budesinsky for measurement of the NMR spectra. V. Petricek gratefully acknowledges the financial support of the Grant Agency of the Czech Republic (GACR 202/00/0645).

References

Allen, F. H. (1986). *Acta Cryst.* B**42**, 512–522.
Altomare, A., Cascarano, G., Giacovazzo, C., Guagliardi, A., Burla, M. C., Polidori, G. & Camalli, M. (1994). *J. Appl. Cryst.* **27**, 435.
Bader, R. F. W. (1990). *Atoms in Molecules: a Quantum Theory*. Oxford: Clarendon Press, Oxford Science Publications.
Bader, R. F. W., Slee, T. S., Cremer, D. & Kraka, E. (1983). *J. Am. Chem. Soc.* **105**, 5061–5068.
Coppens, P. (1997*a*). *X-ray Charge Densities and Chemical Bonding*, ch. 3, pp. 64–67. New York: Oxford University Press.
Coppens, P. (1997*b*). *X-ray Charge Densities and Chemical Bonding*, ch. 5, pp. 105–108. New York: Oxford University Press.
Coppens, P. (1997*c*). *X-ray Charge Densities and Chemical Bonding*, ch. 12, pp. 283–286. New York: Oxford University Press.
Coppens, P. (1998). *Acta Cryst.* A**54**, 779–788.
Coppens, P., Guru Row, T. N., Leung, P., Stevens, E. D., Becker, P. J. & Yang, Y. W. (1979). *Acta Cryst.* A**35**, 63–72.
Dahaoui, S., Jelsch, C., Howard, J. A. K. & Lecomte, C. (1999). *Acta Cryst.* B**55**, 226–230.
Dam, J., Harkema, S. & Feil, D. (1983). *Acta Cryst.* B**39**, 760–766.
Epstein, J., Ruble, J. R. & Craven, M. (1982). *Acta Cryst.* B**38**, 140–149.
Espinosa, E., Lecomte, C., Molins, E., Veintemillas, S., Cousson, A. & Paulus, W. (1996). *Acta Cryst.* B**52**, 519–534.
Espinosa, E., Souhassou, M., Lachekar, H. & Lecomte, C. (1999). *Acta Cryst.* B**55**, 563–572.
Farrugia, L. J. (1997). *J. Appl. Cryst.* **30**, 565.
Frisch, M. J., Trucks, G. W., Schlegel, H. B., Gill, P. M. W., Johnson, B. G., Robb, M. A., Cheeseman, J. R., Keith, T., Petersson, G. A., Montgomery, J. A., Raghavachari, K., Al-Laham, M. A., Zakrzewski, V. G., Ortiz, J. V., Foresman, J. B., Cioslowski, J., Stefanov, B. B., Nanayakkara, A., Challacombe, M., Peng, C. Y., Ayala, P. Y., Chen, W., Wong, M. W., Andres, J. L., Replogle, E. S., Gomperts, R., Martin, R. L., Fox, D. J., Binkley, J. S., Defrees, D. J., Baker, J., Stewart, J. P., Head-Gordon, M., Gonzalez, C. & Pople, J. A. (1995). *Gaussian*94, Revision D.4. Gaussian, Inc., Pittsburgh PA.
Hansen, N. K. & Coppens, P. (1978). *Acta Cryst.* A**34**, 909–921.
Hirshfeld, F. L. (1976). *Acta Cryst.* A**32**, 239–244.
Holy, A. (1993). *Collect. Czech. Chem. Commun.* **58**, 649–674.
Holy, A., Budesinsky, M., Podlaha, J. & Cisarova, I. (1999). *Collect. Czech. Chem. Commun.* **64**, 242–256.
Holy, A., Gunter, J., Dvorakova, H., Masojidkova, M., Andrei, G., Snoeck, R., Balzarini, J. & De Clercq, E. (1999). *J. Med. Chem.* **42**, 2064–2086.
Hooft, R. (1998). *Collect.* Nonius BV, Delft, The Netherlands.
Howard, S. T., Hursthouse, M. B., Lehmann, C. W. & Poyner, E. A. (1995). *Acta Cryst.* B**51**, 328–337.
Ichikawa, M., Gustafsson, T. & Olovsson, I. (1998). *Acta Cryst.* B**54**, 29–34.
Johnson, C. K. (1976). *ORTEP*II. Report ORNL-5138. Oak Ridge National Laboratory, Tennessee, USA.
Klooster, W. T., Swaminathan, S., Nanni, R. & Craven, B. M. (1992). *Acta Cryst.* B**48**, 217–227.
Kuntzinger, S., Dahaoui, S., Ghermani, N. E., Lecomte, C. & Howard, J. A. K. (1999). *Acta Cryst.* B**55**, 867–881.
Martin, A. & Pinkerton, A. A. (1998). *Acta Cryst.* B**54**, 471–477.
Moss, G. R., Souhassou, M., Blessing, R. H., Espinosa, E. & Lecomte, C. (1995). *Acta Cryst.* B**51**, 650–660.
Otwinowski, Z. & Minor, W. (1997). *Methods Enzymol.* **276**, 307–326.
Pearlman, D. A. & Kim, S. (1985). *Biopolymers*, **24**, 327–357.

Pérès, N., Boukhris, A., Souhassou, M., Gavoille, G. & Lecomte, C. (1999). *Acta Cryst.* A**55**, 1038–1048.
Petricek, V. & Dusek, M. (2000). *JANA*2000. Crystallographic Computing System. Institute of Physics, Praha, Czech Republic.
Schaftenaar, G. & Noordik, J. H. (2000). *J. Comput.-Aided Mol. Des.* **14**, 123–134.
Slouf, M. (2001). PhD thesis. Charles University, Czech Republic.
Souhassou, M., Espinosa, E., Lecomte, C. & Blessing, R. H. (1995). *Acta Cryst.* B**51**, 661–668.
Souhassou, M., Lecomte, C., Blessing, R. H., Aubry, A., Rohmer, M., Wiest, R., Benard, M. & Marraud, M. (1991). *Acta Cryst.* B**47**, 253–266.
Spek, A. L. (1990). *Acta Cryst.* A**46**, C-34.
Spackman, M. A., Byrom, P. G., Alfredsson, M. & Hermansson, K. (1999). *Acta Cryst.* A**55**, 30–47.
Stevens, E. D. (1980). *Acta Cryst.* B**36**, 1876–1886.
Stevens, E. D. & Coppens, P. (1980). *Acta Cryst.* B**36**, 1864–1876.
Stevens, E. D., Rys, J. & Coppens, P. (1978). *J. Am. Chem. Soc.* **100**, 2324–2329.
Swaminathan, S., Craven, B. M. & McMullan, R. K. (1985). *Acta Cryst.* B**41**, 113–122.
Volkov, A., Wu, G. & Coppens, P. (1999). *J. Synchrotron Rad.* **6**, 1007–1015.
Volkov, A., Gatti, C., Abramov, Y. & Coppens, P. (2000). *Acta Cryst.* A**56**, 252–258.